Plasma Sci. Technol. **19** (2017) 105501 (8pp) https://doi.org/10.1088/2058-6272/aa7940

Hybrid–PIC simulation of sputtering product distribution in a Hall thruster

Xifeng CAO (曹希峰)[1], **Guanrong HANG** (杭观荣)[2], **Hui LIU** (刘辉)[1], **Yingchao MENG** (孟颖超)[1], **Xiaoming LUO** (罗晓明)[1] **and Daren YU** (于达仁)[1]

[1] Lab of Plasma Propulsion, Mail Box 458, Harbin Institute of Technology (HIT), Harbin 150001, People's Republic of China
[2] Shanghai Institute of Space Propulsion, Shanghai 201112, People's Republic of China

E-mail: thruster@126.com

Received 15 May 2017, revised 8 June 2017
Accepted for publication 12 June 2017
Published 21 August 2017

Abstract

Hall thrusters have been widely used in orbit correction and the station-keeping of geostationary satellites due to their high specific impulse, long life, and high reliability. During the operating life of a Hall thruster, high-energy ions will bombard the discharge channel and cause serious erosion. As time passes, this sputtering process will change the macroscopic surface morphology of the discharge channel, especially near the exit, thus affecting the performance of the thruster. Therefore, it is necessary to carry out research on the motion of the sputtering products and erosion process of the discharge wall. To better understand the moving characteristics of sputtering products, based on the hybrid particle-in-cell (PIC) numerical method, this paper simulates the different erosion states of the thruster discharge channel in different moments and analyzes the moving process of different particles, such as B atoms and B^+ ions. In this paper, the main conclusion is that B atoms are mainly produced on both sides of the channel exit, and B^+ ions are mainly produced in the middle of the channel exit. The ionization rate of B atoms is approximately 1%.

Keywords: Hall thruster, sputtering erosion, hybrid–PIC

(Some figures may appear in colour only in the online journal)

1. Introduction

A Hall thruster is a kind of plasma propulsion device which has been widely used in satellites for attitude control and deep space exploration [1–3]. The structure is shown in figure 1. The ring channel of a Hall thruster consists of an internal and external ceramic wall. The internal and outer coils form a radial magnetic field, and the potential difference between the anode and cathode forms an axial electric field. The electrons are bound by the magnetic field, and the electrons drift along the axial direction under the action of the orthogonal electromagnetic field. The propellant (usually xenon) is electronically ionized to form plasma, and the ions are accelerated to form thrust. The energy of the ions increases significantly as a result of the electric field. High-speed ions have a strong impact on the wall and cause wall erosion [4]. According to the ejection velocity of ions, it can be expected that near the channel exit, the energy of the ions hitting the channel wall is about 200 eV. In contrast, the threshold energy of the Hall thruster's channel wall material, boron nitride (BN) ceramic, is less than 100 eV, and thus the bombardment of incident ions will cause serious sputtering erosion to BN ceramic [5]. This sputtering effect will cause a loss of quality in the Hall thruster's discharge channel, resulting in a lack of protection for some key components, eventually leading to the failure of these components. As a result, the thruster will be unable to continue with further missions and will reach the end of its operation. Therefore, the thruster's operating life is seriously constrained by the sputtering erosion caused by the bombardment of high-energy ions to the discharge wall, which is a key problem for the further development of the Hall thruster.

Much research has been carried out to study the sputtering process. Celik [6] and Yamamoto [7] measured the sputter yield using a spectroscopy technique. Rubin determined the different sputtering rates by measuring the

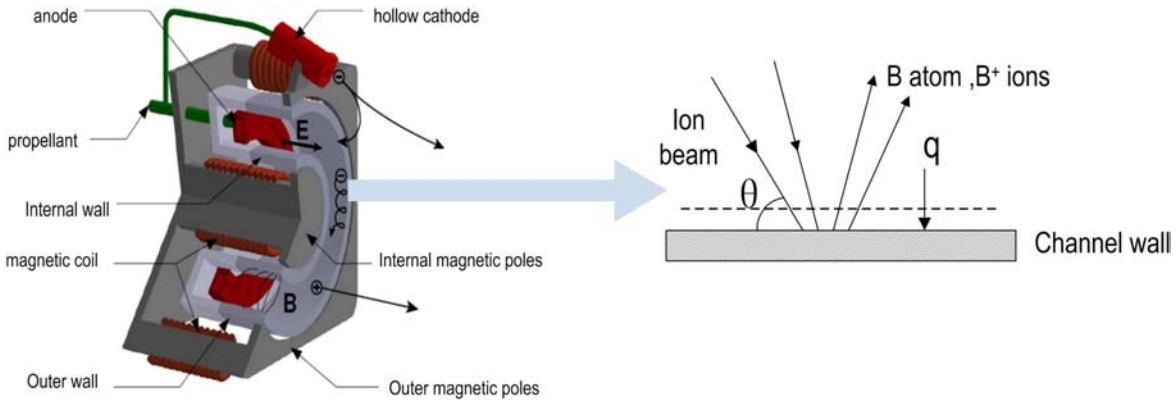

Figure 1. The structure of a Hall thruster and a schematic diagram of the eroding wall.

sediment mass (sputtered particles) by the quartz crystal microbalance. The results showed that the products were mainly B and N atoms rather than compounds [8]. Betz obtained the same conclusion by mass spectrometry [9]. Lee used the CRDS method to measure the density of boron atoms in the inner and the plume regions of a Hall thruster, and boron ion density was estimated by electron temperature and boron atom density. It was estimated that the ionization rate of boron atoms is related to the electron density and temperature, and it is about 1% when the electron density is in the order of magnitude of 10^{17} m^{-3}, which may be larger in the center of the channel [10]. Hargus applied spectrum diagnosis to assess the life duration according to boron atoms in the near field of a BHT-200-X3 Hall thruster [11].

Further, different models have been established to predict the change of macroscopic surface morphology. Manzella predicted an SPT-100 operational lifetime based on a simple analytic model [12]. Fife initially put forward a 2D hybrid particle-in-cell (PIC) to calculate the plasma parameters [13], and Allis [14] and Fernandez [15] modified this model. In addition, many researchers have also studied the influencial factors of lifetime. Garrigue has discussed the influence of the magnetic field configuration on the lifetime of a Hall thruster [16]. Sommier studied the erosion of the Stanford Hall thruster by heavy particle bombardment through the HPHall code [17, 18]. However, there are no systematic reports related to the distribution of sputtering products and the moving characteristics of sputtering products inside the channel and in the plume region.

This paper mainly studies a Hall thruster which uses BN ceramic as a discharge channel wall and Xe as a working propellant. Based on the hybrid–PIC method, the erosion process of the discharge wall in a Hall thruster is analyzed and the moving characteristics of B and B^+, which are generated by sputtering, are simulated. This paper is organized as follows: section 2 describes the hybrid–PIC simulation model. Section 3 discusses the simulation results. Finally, a conclusion is drawn in section 4.

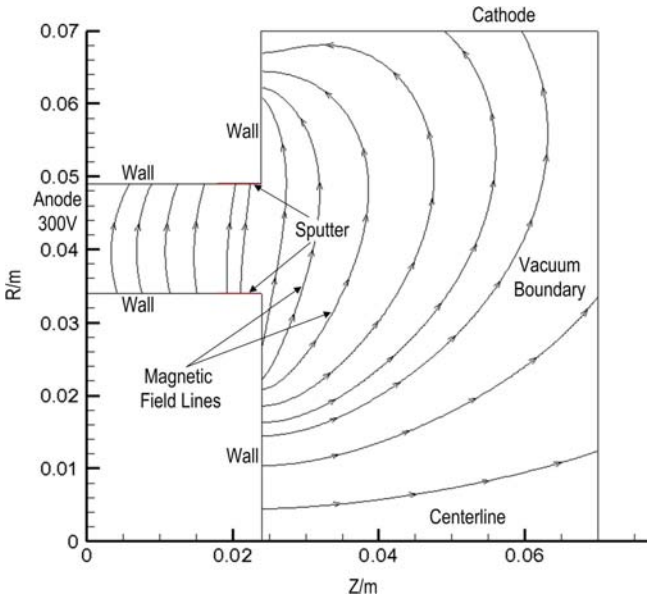

Figure 2. Computational domain and boundary.

2. Simulation model

2.1. Basic physical model

For a typical Hall thruster, the Debye length of the channel is about 0.2 mm, which is much smaller than the channel's characteristic scale (cm order). Therefore, we can use the quasi-neutral hypothesis that the electron density and ion density are equal everywhere. Figure 2 shows the computational domain and boundary. Figure 3 shows the curved magnetic field line, where $\hat{n}$ is the vector perpendicular to the magnetic field line, and $\hat{t}$ is the vector along the magnetic field line.

The treatment of electron motion is mainly considered along the magnetic field direction and perpendicular to the magnetic field direction. The electron diffusion coefficient along the magnetic field lines is assumed to be much larger than that perpendicular to the magnetic field, while ignoring

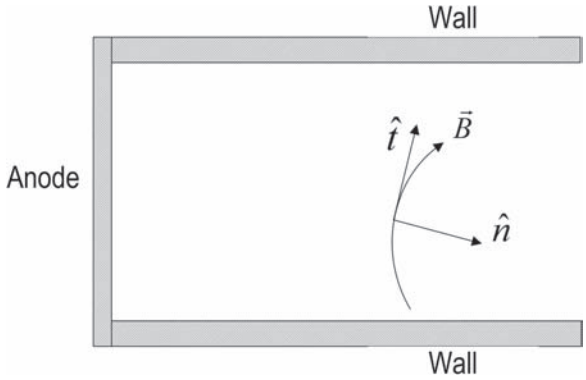

Figure 3. Curved magnetic field line.

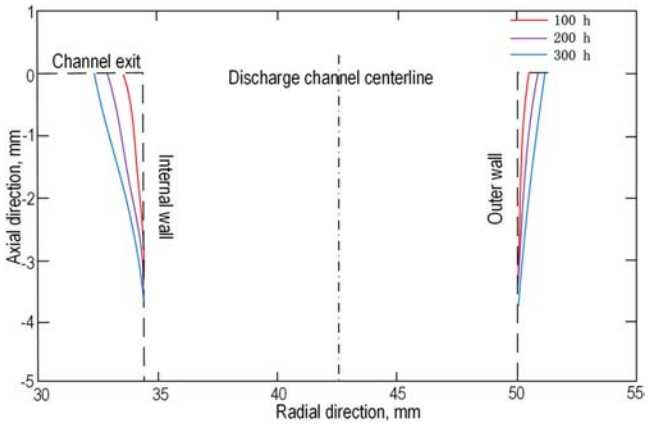

Figure 4. Change of surface morphology in different operating life periods.

the magnetic mirror effect. A balanced equation can be established between the electronic pressure and electric field force along the magnetic field lines:

$$\frac{\partial(n_e k T_e)}{\partial \hat{t}} = e n_e \frac{\partial \phi}{\partial \hat{t}}. \tag{1}$$

In the equation, e is the charge of an electron, n_e is the electronic density, T_e is the electronic temperature, k is the Boltzmann constant, ϕ is the potential.

At the same time, the electron temperature is assumed to be constant along the magnetic field lines; the electron temperature perpendicular to the magnetic field line is solved by using the electron energy equation. λ is the flow function of each magnetic field line, and its gradient is always perpendicular to the magnetic field. The thermalized potential of the magnetic lines is ϕ^*. Therefore:

$$\phi - \frac{kT_e}{e}\ln(n_e) = \phi^*(\lambda). \tag{2}$$

When the thermalized potential of each magnetic field line is determined, the potential at an arbitrary position on the magnetic field line can be obtained from the electron density.

The electron diffusion is assumed to follow the generalized Ohm's law perpendicular to the magnetic field. We can obtain the current density distribution perpendicular to the magnetic field:

$$j_{e,\hat{n}} = -e n_e u_{e,\hat{n}} = \sigma_{e,\perp}\left(E_{\hat{n}} + \frac{1}{e n_e}\frac{\partial p_e}{\partial \hat{n}}\right). \tag{3}$$

where $\sigma_{e,\perp}$ is the conductivity perpendicular to the direction of magnetic field lines. The electron mobility perpendicular to the magnetic field lines is $\mu_{e,\perp}$. Electronic pressure $P_e = n_e k T_e$, electric field $\vec{E} = -\nabla\phi$, and with the thermalized potential formula we can obtain:

$$u_{e,\hat{n}} = \mu_{e,\perp}\left(\frac{\partial \phi^*}{\partial \hat{n}} + \frac{k}{e}(\ln(n_e) - 1)\frac{\partial T_e}{\partial \hat{n}}\right). \tag{4}$$

In the model, we also consider the electrostatic conduction generated by an electron collision with heavy particles and Bohm conduction,

$$\mu_{e,\perp} = \frac{\mu_e}{\beta_e^2} + K_B\frac{1}{16B}. \tag{5}$$

In the equation, $\mu_e = e/\nu_{en} m_e$ is the mobility without considering electron and heavy particle collisions in the magnetic field, $\beta_e = \omega_c/\nu_{en}$ is the electronic Hall parameter, and K_B is the empirical parameter, 0.25.

In the quasi-neutral condition, there is no charge accumulation in the space, and the current is conserved in space. A conservation equation for a current crossing any magnetic field line can be written as

$$I_a = I_e + I_i + I_w \tag{6}$$

where I_i is the ion current, I_e is the electron current in the plasma region, I_w is the total near-wall electron current, where I_i and I_e are equal to the integral of the ion current and the electron current density along the magnetic field lines respectively. Combined with the heat potential equation, we can obtain:

$$\frac{\partial \phi^*}{\partial \lambda} = \frac{-I_a + I_w - 2\pi k\frac{\partial T_e}{\partial \lambda}\int_0^l n_e \mu_{e,\perp} B(\ln(n_e) - 1) r^2 \mathrm{d}s - 2\pi e\int_0^l n_i u_{i,\hat{n}} r \mathrm{d}s}{2\pi e\int_0^l n_e \mu_{e,\perp} B r^2 \mathrm{d}s}. \tag{7}$$

Using the equation, we can find the relationship between the thermalized potential and stream function on each magnetic field line. In the simulation, the potential at each position can be obtained by solving the thermalized potential on the axis of the symmetry axis combined with the thermalized potential equation of the magnetic field lines.

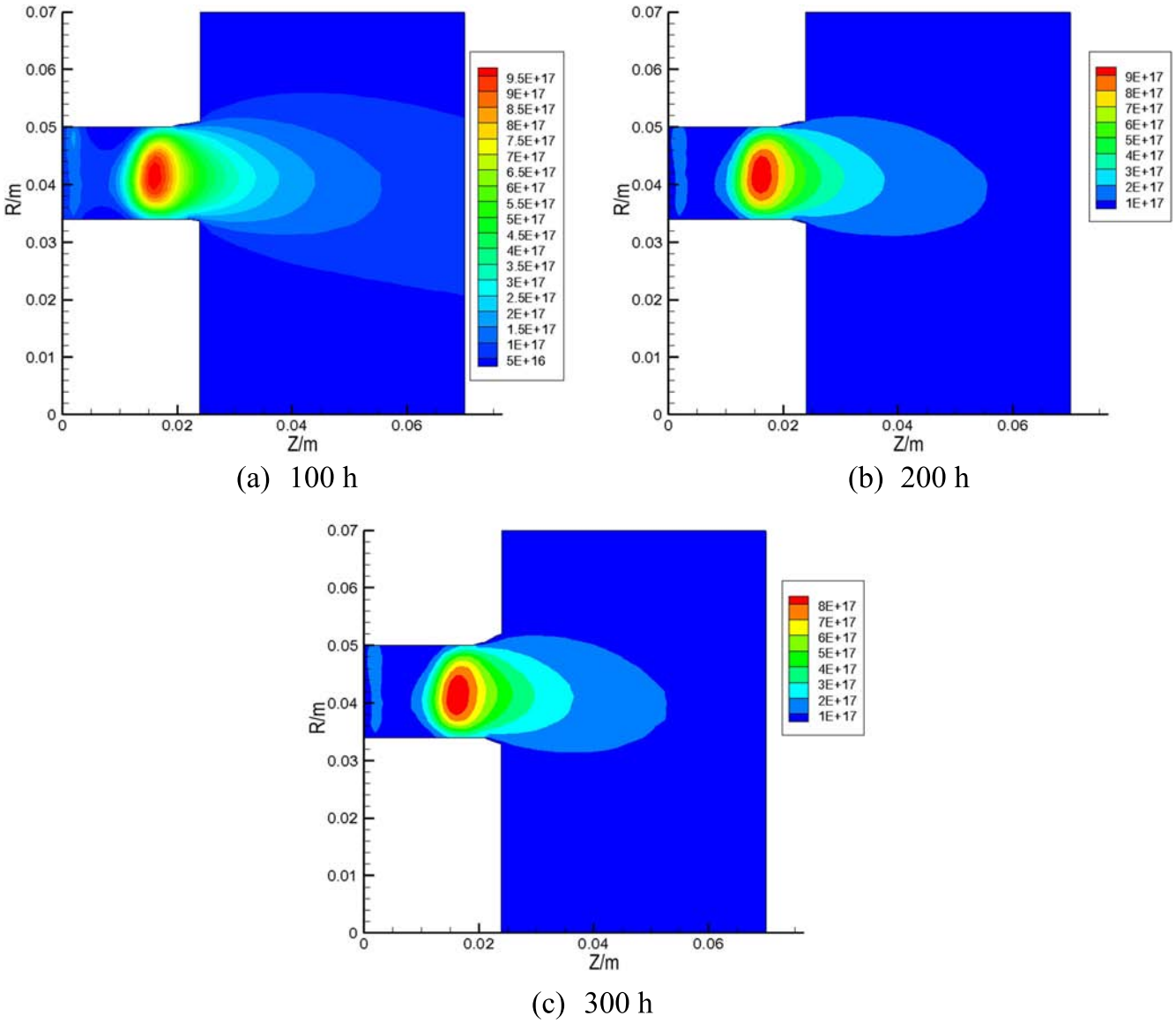

Figure 5. Plasma density distribution in different moments (m^{-3}): (a) 100 h, (b) 200 h, (c) 300 h.

2.2. Domain and boundaries

As shown in figure 2, the computational domain includes the whole inside discharge channel and near-field plume region. The length of the discharge channel is 24 mm, and the width of the channel is 15.7 mm. The length of the near-field plume region is 26 mm. The voltages at the anode and cathode positions are set at 300 V and 0 V.

Neutrals are injected at the anode with a half Maxwell distribution of 300 K. The DSMC method is used to simulate the collision between neutral atoms. When neutral particles have filled the simulation region, electrons are ejected from the cathode at the upper-right boundary. The electron initial velocity distribution is taken to be a half Maxwell distribution.

When particles hit the metallic walls (including the anode and magnetic poles), electrons are deleted, ions lose their charges and are re-emitted as neutrals in a random direction with half their initial kinetic energy. At the centerline, particles are specular reflected. Neutrals hitting the wall are re-emitted at the wall temperature (700 K for the dielectric walls, 0.1 eV for metallic walls) with a half Maxwell distribution. All the particles that move across the free space boundary are removed.

2.3. Ionization model

In a Hall thruster, the main collision types between neutral particles and electrons are elastic collisions, excitation collisions and monovalent ionization collisions. All of them hypothesize that the position and velocity of the background atoms are unchangeable, and the electrons' velocity follows an isotropy distribution while the energy of electrons can be different because of different collision types. Szabo has fitted the curves of different collision cross sections according to experimental data [19]. The collision frequency of each collision type is defined as

$$\omega(\varepsilon_p) = v_p Q(\varepsilon_p) n_a \tag{8}$$

where ε_p refers to the energy of electrons, v_p refers to the velocity of electrons, $Q(\varepsilon_p)$ refers to a certain collision cross section and n_a refers to the present density of the background atoms.

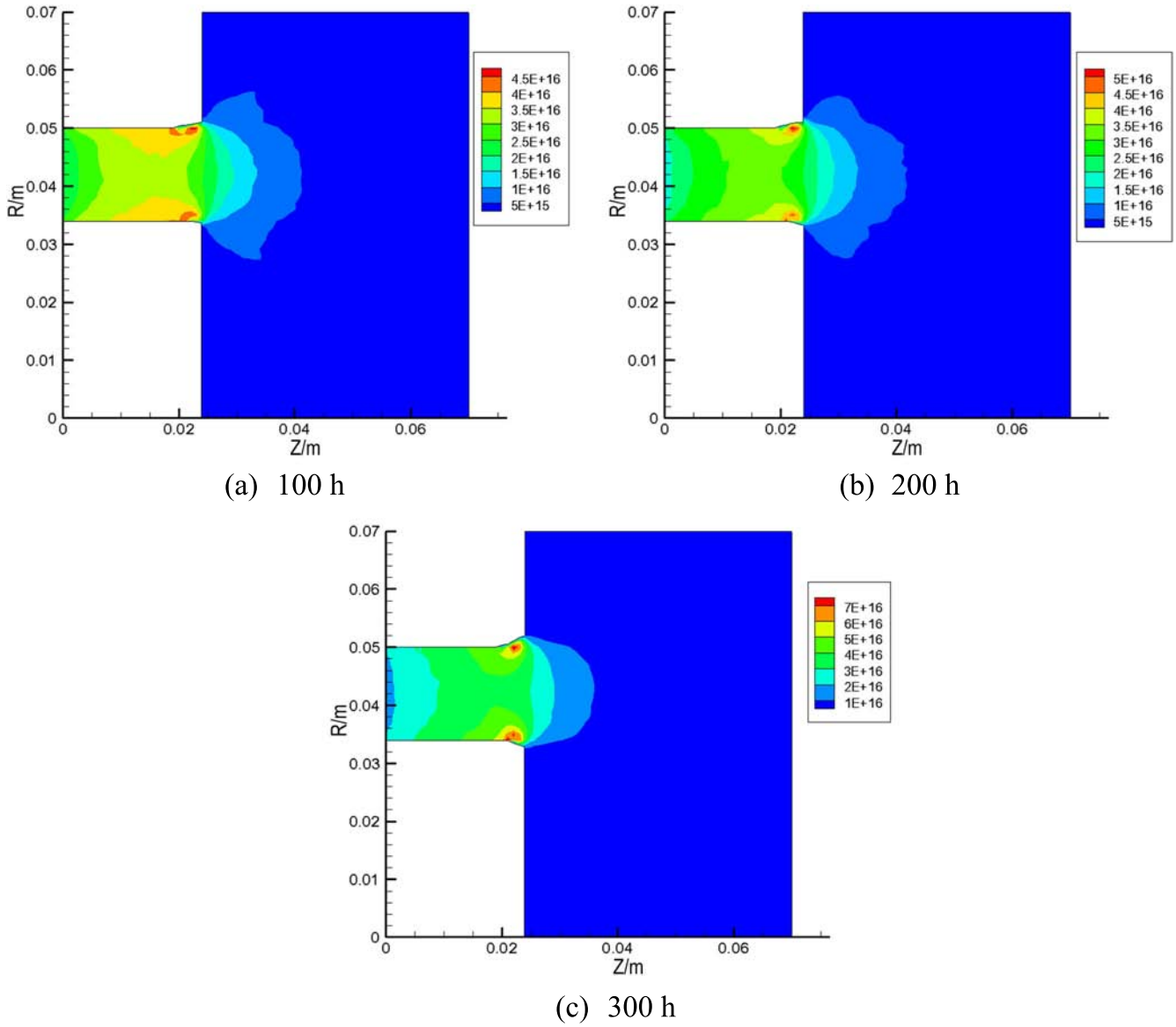

Figure 6. B atom density distribution in different moments (m^{-3}): (a) 100 h, (b) 200 h, (c) 300 h.

Similarly, according to the ionization cross section of B atoms, the B^+ ions' sputtering yield can be obtained and then the moving characteristics of B^+ ions can be simulated. The relationship between the B atom cross section and electron energy can be found in [8].

2.4. Velocity distribution of sputtering B

In the discharge channel of a Hall thruster, the average energy of the ions which can cause sputtering erosion to the BN ceramic discharge wall is above 100 eV, which is determined by the discharge voltage, usually from 100 V–500 V. Therefore, sputtering erosion caused by high-energy ions is the main problem considered here. To continue the research on moving characteristics of sputtering products, the interaction between incident ions and sputtering products should be confirmed and then the distribution function of products sputtering from the discharge wall should be analyzed, which will provide initial conditions to further analyze the motor process of sputtering products.

Smith and Boyd have studied the sputtering effect of Xe+ on BN compounds and have obtained the velocity distribution function through molecular dynamics simulation [20]. By adopting the laser-induced fluorescence method to measure the velocity distribution of sputtering atoms, it can be found that in the direction vertical to the discharge wall, the velocity distribution of sputtering boron atoms satisfies the Sigmund–Thompson function, as is shown in equation (10) [5]:

$$f_{\mathrm{n}}(v_{\mathrm{n}}) \propto \frac{v_{\mathrm{n}}^3}{(v_{\mathrm{n}}^2 + v_{\mathrm{b}}^2)^{3-2m}} \tag{9}$$

where $v_{\mathrm{b}} = 5.25 \times 10^3\ \mathrm{m\ s^{-1}}$ and $m = 0$.

In the direction parallel to the discharge wall, the velocity follows the double Maxwell distribution, as is shown in

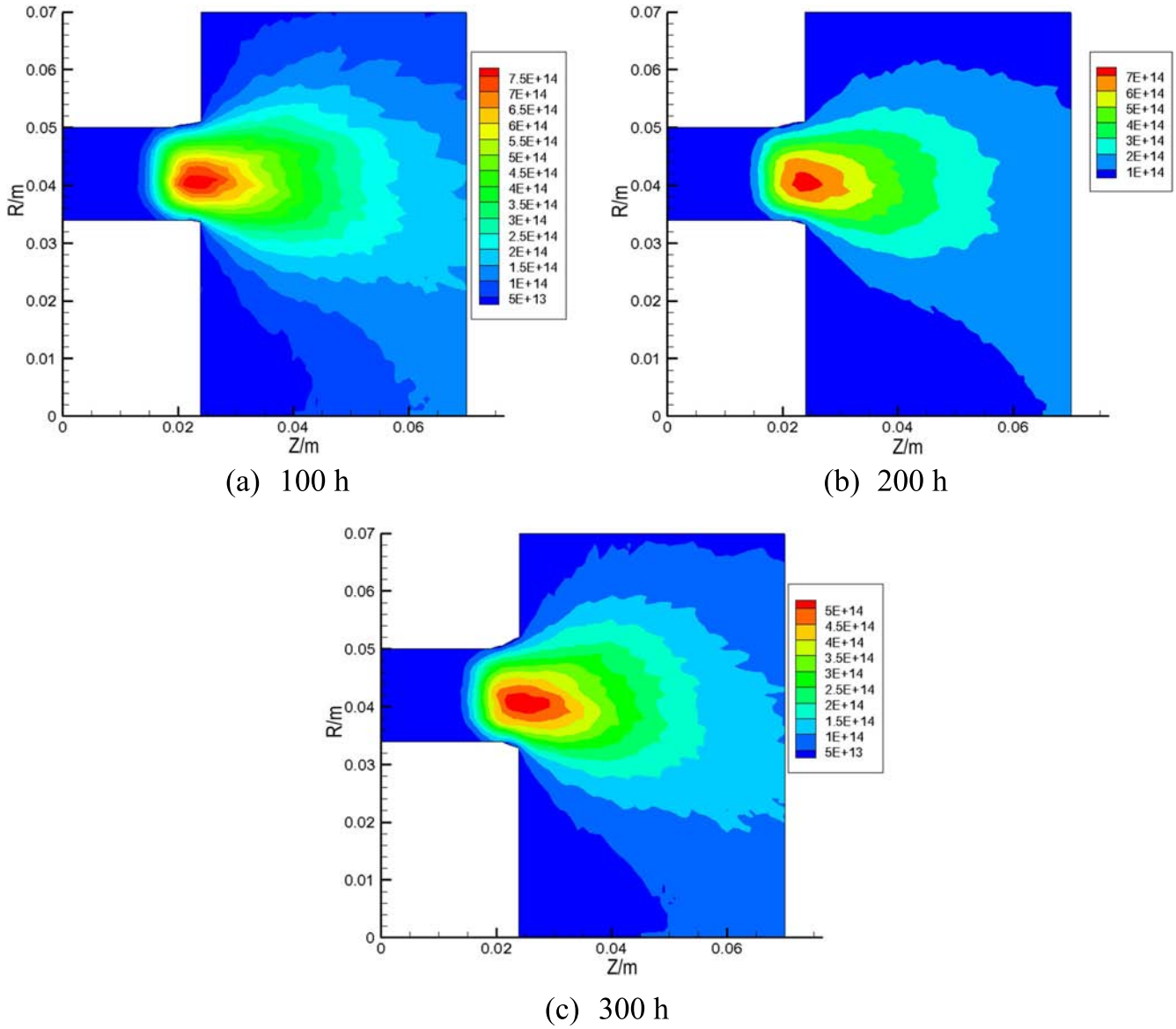

Figure 7. The density distribution of B^+ ions in different moments (m^{-3}): (a) 100 h, (b) 200 h, (c) 300 h.

equation (11):

$$f_t(v_t) \propto \sigma g_1(v_t) + (1 - \sigma) g_2(v_t) \tag{10}$$

$$g_{1,2}(v_t) \propto \sqrt{\frac{m_B}{2\pi k_B T_{i,2}}} \cdot \exp\left[-\frac{m_B(v_t - c_{1,2})^2}{2\pi k_B T_{i,2}}\right] \tag{11}$$

where $\sigma = 0.522$, $c_1 = -1.75 \times 10^3\ \mathrm{m\ s^{-1}}$, $c_2 = -8.56 \times 10^3\ \mathrm{m\ s^{-1}}$, $T_i = 2.62 \times 10^4\ \mathrm{K}$, $T_2 = 3.86 \times 10^4\ \mathrm{K}$ and k_B refers to the Boltzmann constant. In addition, v_n and v_t refer to normal velocity and tangential velocity respectively.

3. Simulation results and analysis

Based on the hybrid–PIC method, the plasma's parameter distributions in different operating life periods are simulated and the evolution process of the plasma's parameter distributions are analyzed. During the simulation, three different moments measured by the experiment are selected. The internal and outer surface morphologies in different operating life periods are shown in figure 4. By comparison, the erosion of the internal wall is more serious because the internal wall is smaller. According to the erosion profile, the erosion rate is calculated, and the sum of the internal and outer wall erosion rate is $2.548\ \mathrm{kg\ s^{-1}}$, $1.635\ \mathrm{kg\ s^{-1}}$ and $4.119\ \mathrm{kg\ s^{-1}}$, corresponding to 100 h, 200 h, and 300 h, so the erosion rate is faster. As demonstrated in figure 2, the discharge voltage is 300 V and the discharge current is 4.5 A. In addition, the anode gas flow rate and the cathode gas flow rate are fixed at $5.3\ \mathrm{mg\ s^{-1}}$ and $0.263\ \mathrm{mg\ s^{-1}}$ respectively.

3.1. Simulation of plasma distribution

Figure 5 is the plasma density distribution in different moments. It can be found that at 100 h, the peak value of the plasma density is $9.5 \times 10^{17}\ \mathrm{m^{-3}}$ and when the thruster

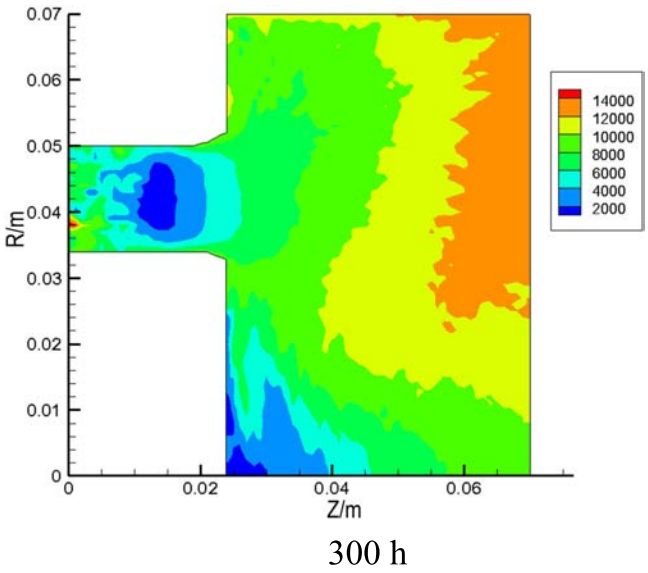

Figure 8. The velocity distribution of B^+ ions at 300 h (m s^{-1}).

reaches 300 h, the peak value reduces to 8×10^{17} m^{-3}. This is because, with the expansion of the surface morphology, the cross section closely located at the ionization zone enlarges as well, which induces a decrease in atom density and electronic density, and will cause the ionization zone to move toward the anode, although the phenomenon is not obvious in the figure. The decrease of atom density and electronic density will cause the ionization rate of atoms to decrease, while the ion beam will be more divergent, and eventually cause the performance of the thruster to diminish, and at the same time, the energy loss related to the interaction between the plasma and discharge wall also decreases.

3.2. Simulation of B atom movement

To figure out the moving characteristics of sputtering products, the B atom density distribution in different operating life periods is simulated as well, which is shown in figure 6. It can be found that the highest sputtering yield occurs at 300 h at about 7×10^{16} m^{-3} because the erosion area is more concentrated at 300 h. In addition, the position of the highest B atom density is located at the exit of the inner wall, which is because the highest BN sputter yield is also located in this area. At the same time, the B atom density is smaller in the middle of the channel due to the ionization of B atoms. The results are consistent with the experimental results in [10], and Dragnea simulated a similar result, but he did not consider the ionization of the boron atom [21]. Besides, B atom density is two or three orders of magnitude less than the density of Xe and in the central area of the exit, B atom density is about 2×10^{16} m^{-3}. During the diffusion of B atoms in the plume area, the B density drops sharply.

3.3. Simulation of B^+ ion movement

On the basis of the B atom density simulation results, the movement of B^+ ions, which are ionized by electrons, are further analyzed. The ionization process of B^+ ions adopts the ionization cross section demonstrated in [5]. After being ionized, the PIC method is used to simulate the B^+ ions, and the B^+ ion density distribution in different moments is shown in figure 7. It can be found that the peak value of B^+ ion density is located at the middle area of the exit. It is because the BN sputter yield is much higher in this field, and the electron temperature is relatively high in this area which ensures the ionization rate of B atoms. When the B^+ ions move from the discharge channel to the plume area under the influence of electric field and pressure difference, the B^+ ion density will decrease significantly. In contrast to the tendency of B atom density, the highest peak value of B^+ ion density occurs at 100 h instead of 300 h. It can be explained by the fact that the ionization region of the boron atom is at the middle area of the exit. Although the peak value of the B atoms is highest at 300 h, the density of the B atoms at the middle area of the exit still decreases. The simulation results show that the ionization rate is about 1%, which is consistent with the results in [10].

The change of the velocity distribution of B^+ ions is not obvious, so figure 8 just shows the velocity distribution of B^+ ions at 300 h. It can be found that the velocity of B^+ ions is much smaller inside the discharge channel, and at the exit and the plume region, B^+ ions will obtain more energy to accelerate. This is because the position of the highest sputtering yield is situated at the exit, and the B atoms are mainly ionized here which is near the plume region. According to the simulation, the maximum accelerating voltage of B^+ ions is about 94.7 V. In other words, the accelerating voltage that B^+ ions can obtain is relatively low, which will induce a greater divergent plume angle. In the protection of the plume, this is a noteworthy problem.

4. Conclusion

Based on the hybrid–PIC method, this paper simulates the plasma parameter distributions in different moments and further analyzes the evolution process of different parameters according to the results. In addition, B atom and B^+ ion distributions are also simulated.

The simulation results show that as the surface erosion morphology becomes larger, the densities of the electrons and atoms decrease and the ionization rate decreases. At the same time, the ion beam becomes more divergent. This will cause the performance of the thruster to diminish.

The simulation results of B atoms and B^+ ions show that the peak value of B atom density reaches the maximum at 300 h, and the main distribution area is located on both sides of the exit. This is because the speed of Xe ions is faster at the exit position and the performance of the impact on the exit wall is most obvious. The distribution of B^+ ions is mainly concentrated in the middle of the channel exit because this position is the main ionization region of B atoms. The speed of the B^+ ions is lower inside the channel, and the speed increases rapidly outside the channel. The plume divergence angle is larger, and this will affect the components on the

satellite. Therefore we need to pay attention to the effect of B atoms and B^+ ions.

References

[1] Diamant K D *et al* 2010 *IEEE Trans. Plasma Sci.* **38** 1052
[2] Kozubskii K N *et al* 2003 *Plasma Phys. Rep.* **29** 251
[3] London A P 1996 A systems study of propulsion technologies for orbit and attitude control of microspacecraft *PhD Thesis* Massachusetts Institute of Technology, Cambridge, MA
[4] Gorshkov O, Shagayda A and Muravlev V 2006 The experience of hall thruster research and development *Proc. of the 57th Int. Astronautical Congress* (Valencia, Spain: AIAA)
[5] Tao L and Yalin A 2010 LIF velocity measurement of sputtered boron atoms from boron nitride target *Proc. of the 46th AIAA/ASME/SAE/ASEE Joint Propulsion Conf. & Exhibit* (Nashville, TN: AIAA)
[6] Celik M, Batishchev O and Martinez-Sanchez M 2010 *Vacuum* **84** 1085
[7] Yamamoto N *et al* 2005 *Rev. Sci. Instrum.* **76** 083111
[8] Rubin B, Topper J L and Yalin A P 2009 *J. Phys.* D **42** 205205
[9] Betz G and Wien K 1994 *Int. J. Mass Spectrom. Ion Process.* **140** 1
[10] Lee B C *et al* 2014 *Rev. Sci. Instrum.* **85** 053111
[11] Hargus W A Jr and Nakles M R 2006 Evolution of the ion velocity distribution in the near field of the BHT-200-X3 hall thruster *Proc. of the 42nd AIAA/ASME/SAE/ASEE Joint Propulsion Conf. & Exhibit* (Sacramento, CA: AIAA)
[12] Manzella D, Yim J and Boyd I 2004 Predicting hall thruster operational lifetime *Proc. of the 40th AIAA/ASME/SAE/ASEE Joint Propulsion Conf. and Exhibit* (Fort Lauderdale, FL: AIAA)
[13] Fife J M 1999 Hybrid-PIC modeling and electrostatic probe survey of hall thrusters *PhD Thesis* Massachusetts Institute of Technology Dept. of Aeronautics and Astronautics, Cambridge, MA
[14] Allis M K *et al* 2004 A comparison of 2D hybrid hall thruster model to experimental measurements *Proc. of the 40th AIAA/ASME/SAE/ASEE Joint Propulsion Conf. and Exhibit* (Fort Lauderdale, FL: AIAA)
[15] Scharfe M K *et al* 2006 *Phys. Plasmas* **13** 083505
[16] Garrigues L *et al* 2003 *Phys. Plasmas* **10** 4886
[17] Sommier E *et al* 2006 Wall erosion in 2D hall thruster simulations *Proc. of the 42nd AIAA/ASME/SAE/ASEE Joint Propulsion Conf. & Exhibit* (Sacramento, CA: AIAA)
[18] Sommier E *et al* 2007 *IEEE Trans. Plasma Sci.* **35** 1379
[19] Szabo J J 2001 Fully kinetic numerical modeling of a plasma thruster *PhD Thesis* Massachusetts Institute of Technology. Dept. of Aeronautics and Astronautics, Cambridge, MA
[20] Smith B D and Boyd I D 2016 *J. Appl. Phys.* **120** 053301
[21] Dragnea H C *et al* 2015 *IEEE Trans. Plasma Sci.* **43** 35